Materials Today Physics 15 (2020) 100273

Contents lists available at ScienceDirect

Materials Today Physics

journal homepage: https://www.journals.elsevier.com/materials-today-physics

2D MoS_2/CuPc heterojunction based highly sensitive photodetectors through ultrafast charge transfer

Z.H Xu [a, 1], L. Tang [b, c, 1], S.W Zhang [b, c], J.Z Li [b, c, d, **], B.L Liu [b, c], S.C Zhao [a, ***], C.J Yu [e], G.D Wei [b, c, *]

[a] College of Materials & Environmental Engineering, Hangzhou Dianzi University, Hangzhou, 310018, PR China
[b] Tsinghua-Berkeley Shenzhen Institute (TBSI), Tsinghua University, Shenzhen, 518055, PR China
[c] Tsinghua Shenzhen International Graduate School, Tsinghua University, Shenzhen, 518055, PR China
[d] Hangzhou Institute for Advanced Study, University of Chinese Academy of Sciences, Hangzhou, 310024, PR China
[e] Department of Mechanical Engineering, University of Houston, Houston, 77004, TX, USA

ARTICLE INFO

Article history:
Received 21 July 2020
Received in revised form
19 August 2020
Accepted 21 August 2020
Available online 10 September 2020

Keywords:
Monolayer MoS_2
CuPc
Photodetector
Charge transfer
p-n junction

ABSTRACT

Photodetectors (PD) with high detectivity, high quantum efficiency and fast response are fundamental units to achieve sensors, imagers, and many others functional optoelectronics. Here we demonstrate high performance vertical stacked 2D MoS_2/CuPc heterojunction based photodetectors with high sensitivity, high external quantum efficiency and ultrafast response time. The functional p-type organic thin film of CuPc was thermally evaporated on n-type two-dimension (2D) MoS_2 monolayer to create an ideal type II heterojunction interface, where ultrafast charge transfer (CT) occur in 16 ps, followed by effective exciton separation and charge collection. As a result, photoresponse time as fast as 436 μs has been obtained for 2D MoS_2/CuPc PDs, as well as a profound responsivity of 3.0×10^3A/W and a detectivity of 2.0×10^{10} Jones with a peak external quantum efficiency (*EQE*) of 483%. This work suggests a feasible route to develop ultrasensitive visible light photodetector by 2D materials.

1. Introduction

High performance photodetectors (PD) are fundamental optoelectronic units for the construction of sensors, imagers, and many others functional devices. Among many performance metrices, high detectivity, high quantum efficiency and fast response are the keys. As one of typical 2D transition metal dichalcogenide materials, the monolayer MoS_2 with remarkable properties such as a direct band gap, strong light-matter interactions and high carrier mobility, exhibits promising application prospects on transistors [1,2], integrated circuits [3], and photodetectors (PD) [4–8]. Typically, the practical application of 2D MoS_2 film for PD devices requires physical construction of other semiconductor materials to form uniform heterojunction structures [9–14]. Functional organic molecules bonded together by weak van der Waals (vdW) have feasible stackablity upon thermal vapor deposition and can readily be deposited on 2D layers to create 2D/organic heterostructures [15]. This unique heteojunction provides advantages of a versatile selection of organic materials and structural design compared with conventional semiconductors that require strict lattice match and necessary semiconductor doping processing [16]. Recent advances have been reported on varied organic molecules to integrate with 2D MoS_2 to enhance their photoresponse such as 3,4,9,10-perylene tetracarboxylic dianhydride (PTCDA) [17], pentacene [18], zinc phthalocyanine (ZnPc) [19] and metal-free phthalocyanine (H_2Pc) [20] et al., enhancing their light-response nature and extending spectral sensitivity.

Previous experimental [17,20] and theoretical works [19] have suggested that the fundamental physics of the excitonic feature is strongly correlated with the hybrid charge transfer (CT) excitons. Femtosecond (fs) to picosecond (ps) CT can occur across thermodynamically favorable 2D/organic interfaces through the functionalization strategy, facilitating the separation of interfacial CT

* Corresponding author. Tsinghua-Berkeley Shenzhen Institute (TBSI), Tsinghua University, Shenzhen, 518055, PR China.
** Corresponding author. Tsinghua-Berkeley Shenzhen Institute (TBSI), Tsinghua University, Shenzhen, 518055, PR China.
*** Corresponding author.
E-mail addresses: lijingzhou1989@sz.tsinghua.edu.cn, lijingzhou1989@sz.tsinghua.edu.cn (J.Z Li), zhaoshichao@hdu.edu.cn (S.C Zhao), weiguodan@sz.tsinghua.edu.cn (G.D Wei).
[1] These two authors are equally contributed.

https://doi.org/10.1016/j.mtphys.2020.100273
2542-5293/

excitons into free electron-hole charges [13]. However, severe interface recombination processes could compete if free charges couldn't be swept off the interface quickly to their respective electrode, inherently limiting realization of fast photoresponse in PD devices. In fact, the on/off switching photoresponse time of the typical 2D MoS_2 is still limited in the range of ms [21,22] for photosensitive PDs. Though the ultrafast response speed of about 3 μs and high detectivity up to 10^{13} Jones has been observed in bulk MoS_2/Si heterojunction PDs with MoS_2 layer as thick as 150 nm [23], it still remains challenging to reach high speed performance in terms of 2D monolayer MoS_2 devices so far. The critical bottleneck remains on the exploration of a new conductive hole transport layer (p-type) to stack with n-type 2D MoS_2, as well as maintaining an idealized energy offset for ultrafast exciton dissociation. The family of the phthalocyanines (Pcs) with low molecular weight and flat organic molecules, exhibits tremendous potential for photoelectric devices [24]. As a typical p-type semiconductor material with decent π-π stacking, copper phthalocyanine (CuPc) exhibits excellent photoelectric response, which has been used as the photoactive layer for holes transport in photoelectric device [25,26].

In this work, the thermally vaporated CuPc film was stacked on pre-patterned monolayer MoS_2 with Au electrodes to create a type II 2D MoS_2/CuPc PD. This unique device stack could ensure Au electrode have a direct contact with monolayer 2D MoS_2 and CuPc respectively, collecting photogenerated electrons from monolayer 2D MoS_2 and holes from CuPc film efficiently. The novel 2D MoS_2/CuPc PD shows a profound responsivity of 3.0×10^3 A/W, a high detectivity of 2.0×10^{10} Jones, a high external quantum efficiency (*EQE*) of 483% and an ultrafast respone time of 436 μs. The obtained photoresponse time is faster by four orders of magnitude compared with that of the pure monolayer MoS_2 PDs. First, the introduced organic CuPc thin layer has effectively smoothed out the surface of 2D MoS_2 layer for multilayer device integration. Second, the created p-n heterojunction of 2D MoS_2/CuPc has significantly suppressed dark current with more than two orders of magnitude lower than pure monolayer MoS_2 PD. Third, CT state has been formed at the interface of 2D MoS_2 and CuPc layers, facilitating ultrafast charge transfer within 16 ps. As a result, fully separated free electron and hole charges under light illumination are effectively swept off through 2D MoS_2 and CuPc layers to their respective electrode, reaching photoresonse as fast as 436 μs. Systematic experimental investigation and fundamental mechanicstic understanding of the 2D inorganic/organic structure and its charge transport illustrate the key aspects of the PD. The results paves a new way for future 2D MoS_2 PD development.

2. Material and methods

The preparation of monolayer MoS_2 was grown in a homemade two-zone CVD furnace with a 1 in. diameter quartz tube. Sulfur powder (100 mg) was located at the upstream zone, and MoO_3 mixed KI (mass ratio 6:1, 5–10 mg) with a facedown SiO_2/Si substrate was placed downstream (8–10 cm). Before growth, the tube was flushed with Ar for 30–40 min to remove the trapped air. Then, the furnace was heated to 780 °C with a heating rate of 40 °C min^{-1} where it is was kept for 1–3 min for the growth of MoS_2 with Ar carrier gas (100 standard cubic centimeter per minute). After that, the furnace was cooled down to room temperature [27]. Then the Au electrodes were evaporated with the mask on monolayer MoS_2. Finally, the CuPc film was stacked on monolayer MoS_2 through physical vapor deposition (PVD) method. In the deposition process, the vacuum of the chamber was below 6×10^{-4} Pa. The deposition rate was ca. 0.1 Å s^{-1}.

Channel length and width were obtained by optical microscopy. The photoluminescence (PL) and Raman spectrum was recorded on Microscopic confocal Raman spectrometer (Horiba LabRAM HR800, America) at room temperature. The atomic force microscopy (AFM) and Kelvin probe force microscopy (KPFM) was taken by Dimension Icon (Bruker Innova,Germany) to obtain the thickness of CuPc film and work function of monolayer MoS_2 and CuPc compared with Au. The transient absorptions (TA) were measured in a standard pump-probe configuration using a LabView-controlled home-build setup with pump of 580 nm (600 μW) and probe of 630 nm (50 μW). All *I–V* and *current-time* curves measurements were carried out with a home-build system at room temperature which consisted of the optical and electrical parts. The optical part includes SC-pro and AOTF-PRO produced by OYSL and can produce 430–1450 nm light which provide the illumination needed by photodetectors. The electrical part consisits of probe and Keithley 2600B and can detect the photodetectors' current. The fast *current-time* curves were measured using the semiconductor analyzing system and probe station at room temperature (Keithley 4200A-SCS, USA, LakeShore, USA).

3. Results

The 2D MoS_2/CuPc PD was fabricated through CuPc film of ca.7 nm thinckness stacking on monolayer MoS_2 with the effective area of 395 μm^2 and the channel distance of 13 μm between two Au electrodes (Fig. S1(a–d)). Fig. 1(a) shows the illustration of 2D MoS_2/CuPc PD device followed fabrication process as shown in Fig. S1(e) and respective transport path for photogerated free electron through 2D MoS_2 and holes through CuPc toward electrodes. The dark and photocurrent were measured with the drain voltage sweeping from −5 to 5 V (V_{DS}) under the 500 nm incident illumination intensity of 143 mW/cm^2. For 2D MoS_2 only device, Fig. 1(b) shows the *I–V* curves exhibiting closely linear and symmetrical features, indicating ohmic contact was formed between monolayer MoS_2 and Au electrodes ($V_G = 0$ V). In contrast, the dark current of 2D MoS_2/CuPc PD was more than two orders of magnitude lower than that of pure monolayer MoS_2 PD. The photocurrent of 2D MoS_2/CuPc PD was slightly higher than that of pure monolayer MoS_2 PD. It is noted that the pure CuPc PD exhibited poor photoelectric response, which was attributed to its intrinsic photoelectric properties as shown in Fig. S2. Compared with pure monolayer MoS_2 and CuPc PDs, the ratio of on/off of 2D MoS_2/CuPc PD has been increased by ca. 100 times as shown in Fig. S3, indicating significant advantage of 2D MoS_2/CuPc PD.

Responsivity time, a direct indicator of response speed of an effective PD, is the time required of current to increase/decrease between the maximum and minimum under on/off laser illumination. Fig. 1(c) shows the rise/decay time is 8.1/15.9 s for pure 2D MoS_2 PD and 4.5/5.3 s for pure CuPc PD under 500 nm laser illumination with 143 mW/cm^2 (Fig. S4). In sharp contrast, the rise time of 2D MoS_2/CuPc PD is 436 μs (Fig. 1(d)), which is more than four orders of magnitude faster than that of pure 2D MoS_2 devices, indicating that the ultrafast responsivity time has been obtained.

The responsivity (R) and detectivity (D^*) are performance key indicators of PD and calculated according to

$$\mathrm{R} = \frac{I_{light} - I_{dark}}{\mathrm{PA}} \tag{1}$$

$$D^* = \frac{R}{\sqrt{\frac{2eI_{dark}}{A}}} \tag{2}$$

where I_{light} and I_{dark} were light and dark currents, respectively. P

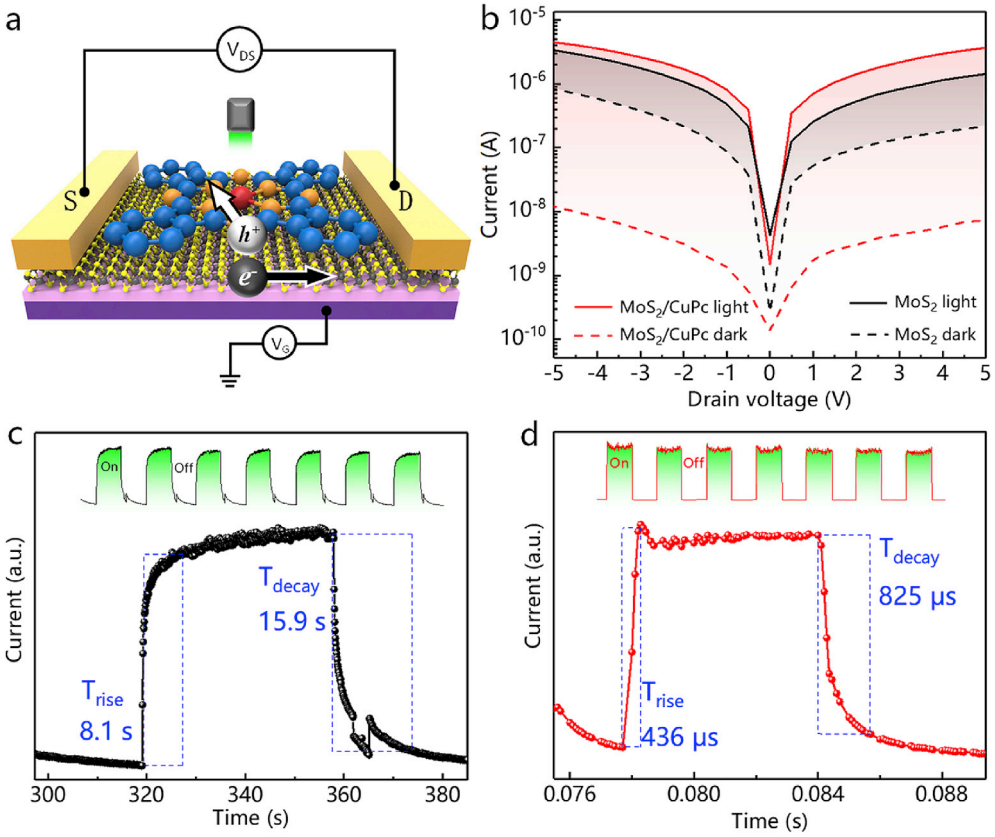

Fig. 1. (a) The illustration of 2D MoS_2/CuPc PD. (b) The I–V curves corresponding to pure monolayer MoS_2 and 2D MoS_2/CuPc PDs. The response time (rise and decay) of pure MoS_2 monolayer (c) and 2D MoS_2/CuPc (d) PDs. Inserts: The corresponding PDs *current-time* curves.

and *A* represented the power density of excitation light and channel effective area of PD, respectively. The *e* is the electronic charge. The channel effective area was 395 μm^2. Fig. 2(a) shows the *I–V* curves of 2D MoS_2/CuPc PD under the laser light of 500 nm with varied power intensities (V_{DS} = 15 V and V_G = 0 V), exhibiting the gradually increased photocurrent with incident power. Fig. 2(b) shows *R* and *D** reach to 3.0 × 10^{3}A/W and 2.0 × 10^{10} Jones at incident power of 0.28 mW/cm^2, repspectively, then they decreases with

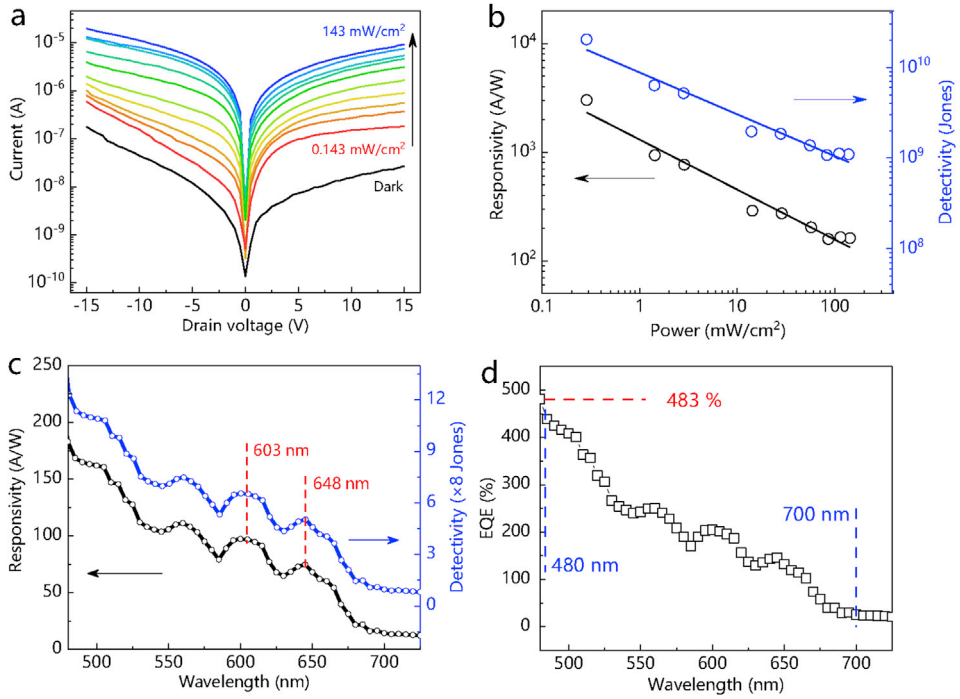

Fig. 2. (a) The *I–V* curves of 2D MoS_2/CuPc PD dependence on power. Responsivity and Detectivity of 2D MoS_2/CuPc PD dependence on power (b) and wavelength (c), respectively. (d) The *EQE* of 2D MoS_2/CuPc PD dependence on wavelength.

power intensity. The responsivity and detectivity of this device linearly decreases with the laser power, which indicates photogenerated excitons are effectively dissociated and separated into free electron and hole charges. With the incident light scanning from 450 nm to 750 nm at fixed power of 143 mW/cm^2, there were two obvious peaks located at 603 nm and 648 nm in Fig. 2(c) which are corresponding to absorption of A and B excitons in monolayer MoS_2[28]. Fig. 2(d) shows the external quantum efficiency (*EQE*) dependence on wavelength of excitation light, which was calculated by

$$EQE = \frac{Rhc}{e\lambda} \tag{3}$$

where *h* represents Planck constant, c represents the speed of light and represents the excitation light wavelength. The maximum of *EQE* was up to 483% at 480 nm and the 2D MoS_2/CuPc PD exhibits broad visible light spectral response.

4. Discussion

As the typical p-type semiconductor of small organic molecule with the hole mobility of 0.7 cm^2 V^{-1} s^{-1} [29], CuPc is stacked on monolayer MoS_2 of n-type semiconductor to architect the vertical p-n heterojunction [30]. Extra electron diffuses from MoS_2 to CuPc and holes from CuPc to MoS_2 until local charge concentration were equalized at the depletion zone [31] and the built-in electric field was formed [32]. There are A exciton states which include A^- trions and A^0 excitons in monolayer MoS_2. The A^- trions consist of two electrons and one hole, and A^0 excitons consisted of one electron-hole pair [28]. Under light illumination, there are more and more photogenerated electron-hole pairs in monolayer MoS_2 and they are more likely to bond with one extra electron to form A^- trion. On the other hand, if no abundant electrons available, they are more likely to form the neutral exciton A^0 [33]. Meanwhile, the thermal activation (E_a) of A^- trions is lower than that of A^0 excitons, [34,35] which could be estimated by temperature-dependent PL spectra to identify types of excitons. For comparison, both pure monolayer MoS_2 and 2D MoS_2/CuPc layers were consistently measured as shown in Fig. 3(a). Fig. 3(b) shows the integrated PL intensities dependence on $1/k_bT$ which was calculated from temperature (T) and Boltzmann constant (k_b). The integrated PL intensities of pure monolayer MoS_2 decreased rapidly with temperature increasing, compared to 2D MoS_2/CuPc heterojunction. The solid lines were fitted with the equation [22,36].

$$I_T = \frac{I_0}{1 + Ae^{\left(-\frac{E_a}{k_bT}\right)}} \tag{4}$$

where I_T represents the measured integrated PL intensities; e is natural constant; k_b is the boltzmann constant; and T represents the measured temperature. I_0 and A are the fitting parameters. The fitting results shows that the E_a of pure monolayer MoS_2 is 38.6 ± 18.1 meV which agrees well with the E_a of A^- trions in monolayer MoS_2, and the E_a of 2D MoS_2/CuPc heterojunction is increased to 62.7 ± 6.9 meV which is attributed to A^0 excitons [33,37]. Therefore, excess electrons generated from light excitation of PL measurement could been effectively drifted away from the MoS_2 to CuPc layer by the built-in electric field, and more electrical neutral A^0 exciton exist in 2D MoS_2/CuPc, indicating an ideal stack

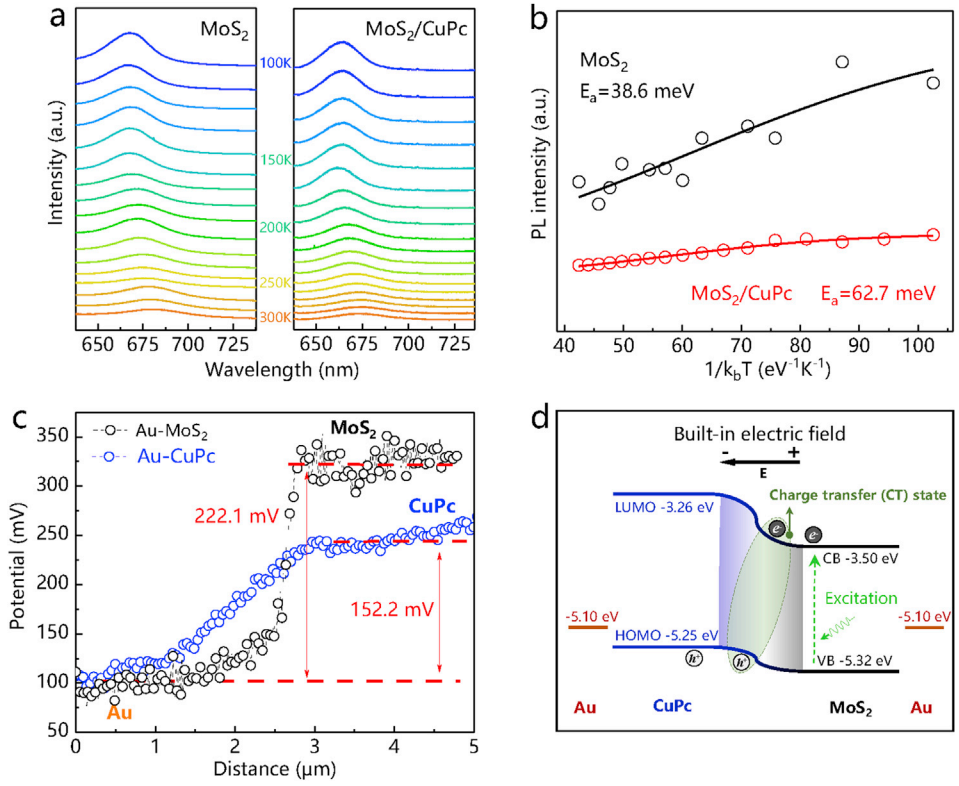

Fig. 3. (a) The PL spectra dependence on temperature corresponding to pure monolayer MoS_2 and 2D MoS_2/CuPc layers. (b) Integrated PL intensities of pure monolayer MoS_2 and 2D MoS_2/CuPc layers as function of $1/k_bT$. The dots represent measured data and the solid lines represent fitting curves by the equation as shown in the text. Black dots and solid line represent pure monolayer MoS_2, and red dots and solid line represent 2D MoS_2/CuPc layers. (c) The potential difference of CuPc and monolayer MoS_2 compared with Au which were tested by Kelvin probe force microscopy (KPFM). (d) Band diagram for CuPc and monolayer MoS_2. Black and white dots represent electrons and holes, respectively.

for effective exciton dissociation.

The Highest Occupied Molecular Orbital (HOMO) level of CuPc and valence band level of monolayer MoS_2 are measured through work function and potential difference with Au which were tested by Kelvin probe force microscopy (KPFM) as shown in Fig. 3(c) and the energy band alignment of 2D MoS_2/CuPc diodes is shown in Fig. 3(d). The lowest unoccupied molecular orbital (LUMO) of CuPc and conduction band level of monolayer were calculated with the PL and absorption spectra, respectively (Fig. 4(a) and Fig. S5). The incorporation of the CuPc layer has created an energy favorable p-n junction and the built-in potential could effectively block the electrons or holes leaked from Au electrodes in dark condition, leading to significantly suppressed dark current.

The PL spectra in Fig. 4(a) at room temperature shows the A exciton-states emitting of monolayer MoS_2 located at 680.1 nm, including A^- trions and A^0 excitons [38]. The PL peak of 2D MoS_2/CuPc heterojunction has slight blueshift to 673.8 nm and its intensity decreased obviously due to the increased proportion of A^0 excitons. The results suggest the existence of the charge CT state of the heterojunction structure as shown in Fig. 3(d), where the CT state has provided an intermediate state to dissociate coulombically bonded excitons. As a result, photogenrated electrons get less chance to accumulate at the interface and transport fast to its electrode, which is consistent with the higher E_a of 2D MoS_2/CuPc heterojunction as shown in Fig. 3(b). In the meantime, electron mobility of monolayer MoS_2 could be three orders of magnitude higher than that of CuPc film [39,40], therefore, the electrons mainly transport to Au electrode through monolayer MoS_2. Simultaneously, the absorption of CuPc could contribute the photocurrent generation with exciton dissociated effectively at the interfaces, increasing the photocurrent generation as shown in Fig. 1(b).

To further investigate the CT state, the transient absorption spectrum (TAS) were measured on monolayer MoS_2, CuPc and 2D MoS_2/CuPc heterojunction with pump of 580 nm and probe of 630 nm as shown in Fig. 4(b). The $\Delta A/A$ was calculated from $\Delta A=(A_{off}-A_{on})/A_{off}$, where A_{off} and A_{on} was absorption without and with pump, respectively. Fig. 4(b) shows that the decay time of the exciton-state absorption in monolayer MoS_2 and Q-band absorption in CuPc are 48 ps and 74 ps, respectivity. For the 2D MoS_2/CuPc heterojunction, the probe of 630 nm is consistence with the exciton-state absorption of monolayer MoS_2 and Q-band absorption of CuPc. The positive signal shows the decay time of 16 ps (T_1), which is attributed to the ground-state bleaches in monolayer MoS_2 and CuPc [19,41]. The kinetic fitting of TA spectrum has indicated that ultrafast CT occurred at 2D MoS_2/CuPc heterojunction interface, where CT could effecitively be dissociated into electron-hole pairs [42]. Therefore, the energy favorable CuPc layer has facilitated the CT with MoS_2 and ultrafast exciton dissociation has been obtained, followed by effective charge separation and collection. Consistently, photo respone time of 2D MoS_2/CuPc PD as fast as 436 μs has been realized as shown in Fig. 1(d), indicating an ideal device architecture for high performance PDs.

Fig. 4(c) exhibits the *current-time* curves of the 2D MoS_2/CuPc PD dependence on laser power under the laser of 500 nm ($V_{DS}=15$ V, $V_G=0$ V). The photocurrent increases with the increase of the laser power, due to more free carriers are generated and transport to Au electrodes under higher power laser illumination. The PD exhibits fast response time under different power. It is noted that the photocurrent under 101 mW/cm^2 and below are horizontality after increasing rapidly. However, the photocurrent under

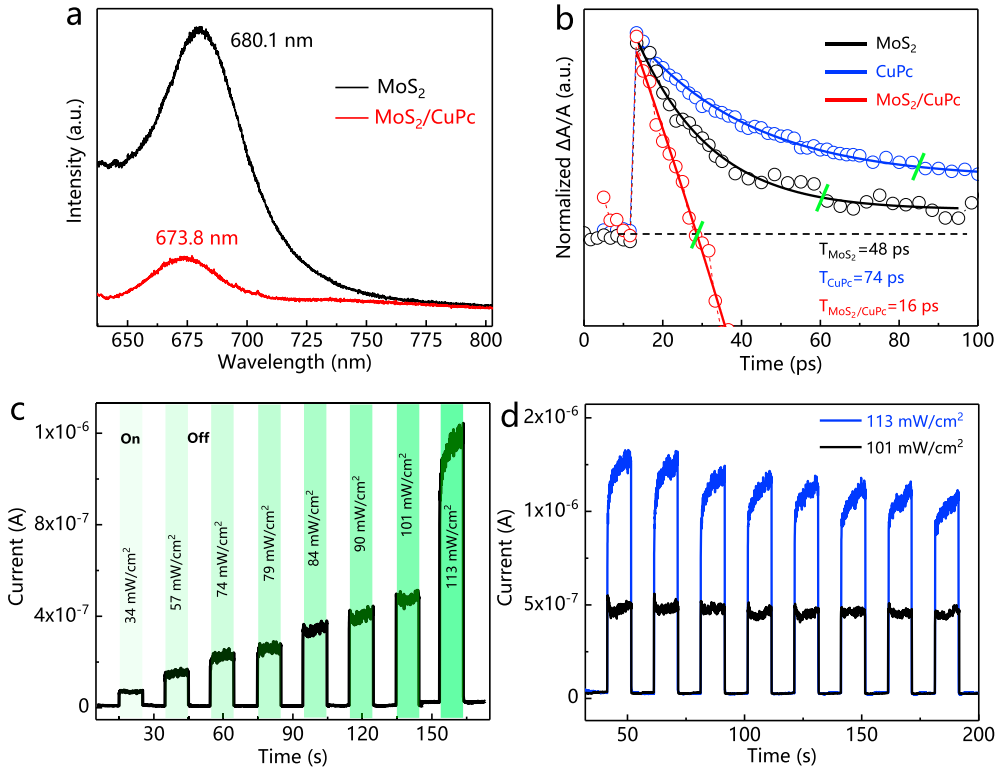

Fig. 4. (a) The PL spectra corresponding to pure monolayer MoS_2 and 2D MoS_2/CuPc heterojunction. (b) The normalized transient absorption (TA) of monolayer MoS_2, CuPc and 2D MoS_2/CuPc heterojunction with pump of 580 nm (600 μW) and probe of 630 nm (50 μW), respectively. (c) The *current-time* curves of 2D MoS_2/CuPc PD dependence on power at laser of 500 nm. (d) The *current-time* curves of 2D MoS_2/CuPc PD under the powder of 101 and 113 mW/cm^2.

113 mW/cm^2 is obliquely upward to peak value after increasing rapidly (Fig. 4(d)), showing the "climbing phenomenon" near the maximum. As the laser power increases, more and more photo-generated carriers are accumulated at the interface due to unbalanced electron and hole mobilities in monolayer MoS_2 and CuPc, and non-radiative recombination occurs. Free carriers get slower to reach the electrode, which results in the climbing rising curve. It is worth mentioning that more conductive layers to stack with 2D MoS_2 may lead to even faster photoresponse.

5. Conclusions

In summary, a high-performance 2D MoS_2/CuPc PD has been developed with the response time, responsivity, detectivity and *EQE* of 436 μs, 3.0×10^3A/W, 2.0×10^{10} Jones and 483%, respectively. Compared to pure monolayer MoS_2 PD, the response rise time has been reduced by more than four orders of magnitude. Due to the unique heterojunction device architecture, the formed build-in electric field at the interface of MoS_2 and CuPc has significantly suppressed the dark current. The energy favorable CuPc layer facilitates the CT state with the MoS_2. The ultrafast CT within 16 ps leads to the short photoresponse time of 436 μs for the 2D MoS_2/CuPc PD. It is noted that the "climbing phenomenon" of the photocurrent under higher light intensity occurs, which suggests that the non-radiative recombination of free carriers caused by unbalanced electron and hole mobilities in the monolayer MoS_2 and CuPc still limit further performance enhancement. This work sheds light on the development of high-performance 2D inorganic/organic PDs based on monolayer MoS_2.

Credit author statement

Z.H. Xu, J. Z. Li and G.D. Wei did the concept proposal; Z. H. Xu and J.Z. Li did device growth and measurement; L. Tang and B. L. Liu, 2D MoS_2 growth and characterization; S.W. Zhang, S.C. Zhao, C.J. Yu, G. D. Wei, discussion and corrections.

Declaration of competing interest

The authors declare that they have no known competing financial interests or personal relationships that could have appeared to influence the work reported in this paper.

Acknowledgement

This work was supported by the Natural Science Foundation of China, China (Grant Number: 03012800001).

Appendix A. Supplementary data

Supplementary data to this article can be found online at https://doi.org/10.1016/j.mtphys.2020.100273.

References

[1] L. Xie, M. Liao, S. Wang, H. Yu, L. Du, J. Tang, J. Zhao, J. Zhang, P. Chen, X. Lu, G. Wang, G. Xie, R. Yang, D. Shi, G. Zhang, Adv. Mater. 29 (2017) 1702522.
[2] J. Chang, L.F. Register, S.K. Banerjee, Appl. Phys. Lett. 103 (2013) 223509.
[3] B. Radisavljevic, M.B. Whitwick, A. Kis, Acs Nano 5 (2011) 9934.
[4] F. Liao, J. Deng, X. Chen, Y. Wang, X. Zhang, J. Liu, H. Zhu, L. Chen, Q. Sun, W. Hu, J. Wang, J. Zhou, P. Zhou, D. Zhang, J. Wan, W. Bao, Small 16 (2019) 1904369.
[5] D. Dumcenco, D. Ovchinnikov, K. Marinov, P. Lazi, M. Gibertini, N. Marzari, O.L. Sanchez, Y. Kung, D. Krasnozhon, M. Chen, S. Bertolazzi, P. Gillet, A.F. Morral, A. Radenovic, A. Kis, Acs Nano 9 (2015) 4611.
[6] K.F. Mak, C. Lee, J. Hone, J. Shan, T.F. Heinz, Phys. Rev. Lett. 105 (2010) 136805.
[7] L LV, F. Zhuge, F. Xie, X. Xiong, Q. Zhang, N. Zhang, Y. Huang, T. Zhai, Nat. Commun. 10 (2019) 3331.
[8] X. Zhang, J. Jiang, A.A. Suleiman, B. Jin, X. Hu, X. Zhou, T. Zhai, Adv. Funct. Mater. 29 (2019) 1906585.
[9] Y. Xue, Y. Zhang, Y. Liu, H. Liu, J. Song, J. Sophia, J. Liu, Z. Xu, Q. Xu, Z. Wang, J. Zheng, Y. Liu, S. Li, Q. Bao, ACS Nano 10 (2016) 573–580.
[10] Y. Liu, N.O. Weiss, X. Duan, H.C. Cheng, Y. Huang, X.F. Duan, Nat. Rev. Mater. 1 (2016) 160429.
[11] L. Li, W. Han, L. Pi, P. Niu, J. Han, C. Wang, B. Su, H. Li, J. Xiong, Y. Bando, T. Zhai, Info 1 (2019) 54–73.
[12] X. Zhou, X. Hu, S. Zhou, H. Song, Q. Zhang, L. Pi, L. Li, H. Li, J. Lv, T. Zhai, Adv. Mater. 30 (2018) 1703286.
[13] Y. Fang, X. Hu, W. Zhao, J. Pan, D. Wang, K. Bu, Y. Mao, S. Chu, P. Liu, T. Zhai, F. Huang, J. Am. Chem. Soc. 141 (2019) 790–793.
[14] P. Luo, F. Zhuge, Q. Zhang, Y. Chen, L. Lv, Y. Huang, H. Lia, T. Zhai, Nanoscale Horiz 4 (2019) 26–51.
[15] J. Yan, Y. Hao, Y. Cui, J. Zhang, Y. Zou, W. Zhang, G. Yu, J. Zheng, W. Xu, D. Zhu, J. Mater. Chem. C. 6 (2018) 12976.
[16] Y. Zhao, I. Stefano, P. Samorì, Adv. Optical Mater. 7 (2019) 1900286.
[17] X. Liu, J. Gu, K. Ding, D. Fan, X. Hu, Y.W. Tseng, Y.H. Lee, V. Menon, S.R. Forrest, Nano Lett. 17 (2017) 3176.
[18] X. Xie, X. Liu, Q. Fang, W. Fang, G. Cui, J. Phys. Chem. 123 (2019) 7693.
[19] T.R. Kafle, B. Kattel, P. Yao, P. Zereshki, H. Zhao, W. Chan, J. Am. Chem. Soc. 141 (2019) 11328.
[20] N. Mutz, S. Park, T. Schultz, S. Sadofev, S. Dalgleish, L. Reissig, N. Koch, E.J.W. List-Kratochvil, S. Blumstengel, J. Phys. Chem. C 124 (2020) 2837–2843.
[21] S.W. Shen, D.G. Chen, I.T. Chen, K.H. Chang, C.W. Lee, C.T. Fang, Y. Chen, W.T. Chuang, Y.H. Lee, Y. Wu, P. Chou, C.I. Wu, Adv. Optical Mater. 4 (2020) 1902179.
[22] Y. Huang, F. Zhuge, J. Hou, L. Lv, P. Luo, N. Zhou, L. Gan, T. Zhai, ACS Nano 12 (2018) 4062.
[23] L. Wang, J. Jie, Z. Shao, Q. Zhang, X. Zhang, Y. Wang, Z. Sun, S.T. Lee, Adv. Funct. Mater. 25 (2015) 2910.
[24] S. Riad, Thin Solid Films 370 (2000) 253.
[25] L. Zhang, Y. Yang, H. Huang, L. Lyu, H. Zhang, N. Cao, H. Xie, X. Gao, D. Niu, Y. Gao, J. Phys. Chem. C 119 (2015) 4217.
[26] F. Takeshi, K. Kobayashi, Y. Hirofumi, M. Kazumi, J. Appl. Phys. 95 (2004) 4742.
[27] L. Tang, L. Tao, Y. Luo, S. Feng, Z. Cai, H. Zhang, B. Liu, H.M. Cheng, ACS Nano 14 (2020) 4646–4653.
[28] K.F. Mak, K. He, C. Lee, G.H. Lee, J. Hone, T.F. Heinz, J. Shan, Nat. Mater. 12 (2013) 207–211.
[29] J. Gao, J.B. Xu, M. Zhu, N. Ke, D. Ma, J. Phys. D Appl. Phys. 40 (2007) 5666.
[30] Y. Koshiba, T. Ohnishi, M. Morimoto, M. Misaki, T. Fukushima, K. Ishida, Mol. Cryst. Liq. Cryst. 653 (2017) 157–163.
[31] A. Janaa, K. Kumari, A. Deya, P.S.S. Reddy, B. Biswas, B. Gupta, S.K. Sarkar, Sens. Actuators, A A. 299 (2019) 111574.
[32] N. Shibata, S.D. Findlay, H. Sasaki, T. Matsumoto, H. Sawada, Y. Kohno, S. Otomo, R. Minato, Y. Ikuhara, Sci. Rep. 5 (2015) 10040.
[33] A. Arora, T. Deilmann, T. Reichenauer, J. Kern, S.M. Vasconcellos, M. Rohlfing, R. Bratschitsch, Phys. Rev. Lett. 123 (2019) 167401.
[34] C. Zhang, A. Johnson, C.L. Hsu, L.J. Li, C.K. Shih, Nano Lett. 14 (2014) 2443.
[35] N. Saigal, V. Sugunakar, S. Ghosh, Appl. Phys. Lett. 108 (2016) 132101.
[36] P. Jing, J. Zheng, M. Ikezawa, X. Liu, S. Lv, X. Kong, J. Zhao, Y. Masumoto, J. Phys. Chem. C 113 (2009) 13545.
[37] T.C. Berkelbach, M.S. Hybertsen, D.R. Reichman, Phys. Rev. B 88 (2013): 045318.
[38] A. Splendiani, L. Sun, Y. Zhang, T. Li, J. Kim, C.Y. Chim, G. Galli, F. Wang, Nano Lett. 10 (2010) 1271.
[39] N. Huo, Y. Yang, Y. Wu, X. Zhang, S.T. Pantelidese, G. Konstantatos, Nanoscale 10 (2018) 15071.
[40] M. Kitamura, T. Imada, S. Kako, Y. Arakawa, Jpn. J. Appl. Phys. 43 (2004) 2326.
[41] S. Padgaonkar, S.H. Amsterdam, H. Bergeron, K. Su, T.J. Marks, M.C. Hersam, E.A. Weiss, J. Phys. Chem. C 123 (2019) 13337.
[42] S.H. Amsterdam, T.K. Stanev, Q. Zhou, A.J.T. Lou, H. Bergeron, P. Darancet, M.C. Hersam, N.P. Stern, T.J. Marks, Acs Nano 13 (2019) 4183.